J Therm Spray Tech
https://doi.org/10.1007/s11666-021-01223-w

PEER REVIEWED

Plasma-Sprayed Graphene Nanosheets/ZnO/Al_2O_3 Coatings with Highly Efficient Microwave Absorption Properties

Xin Liu[1] · Xiaolong Lu[1] · Ying Song[1] · Shaoqiu Xia[1] · Ronghao Ren[1] · Yongguang Wang[1] · Dong Zhao[1] · Mingdi Wang[1]

Submitted: 2 December 2020 / in revised form: 25 May 2021 / Accepted: 28 May 2021

Abstract Graphene nanosheets (GNSs)/ZnO/Al_2O_3 composite coatings with different GNSs content were prepared by air plasma spraying technique. The scanning electron microscope results show that the GNSs were homogeneously dispersed in the powders and coatings. The influence of different GNSs content on complex permittivity and microwave absorption properties have been systematically investigated at the frequency range from 8.2 to 12.4 GHz. The complex permittivity of the coating was improved with the increase in GNS content, due to the high conductivity and polarization loss of GNS. The GNSs/ZnO/Al_2O_3 coating with 15 wt.% GNSs in the thickness of 1.82 mm presented the most prominent microwave absorption properties, which exhibited strong absorption (minimum reflection loss of −45 dB) and the reflection loss ≤ -10 dB bandwidth at the frequency range of 11.2-12.0 GHz. Meanwhile, the hardness of the coating increased from 914.2 $HV_{0.2}$ to 1057.3 $HV_{0.2}$ with the introduced 15 wt.% GNSs. These results suggest that GNS can be a promising nanofiller to simultaneously improve the microwave absorption properties and mechanical properties of absorbing coatings.

✉ Dong Zhao
zhaodong@suda.edu.cn

✉ Mingdi Wang
wangmingdi@suda.edu.cn

Xin Liu
liuxin0433@163.com

[1] School of Mechanical and Electrical Engineering, Soochow University, 8 Jixue Road, Suzhou 215021, People's Republic of China

Keywords complex permittivity · graphene · microwave absorption · plasma spraying

Introduction

With the rapid advancement in wireless communication, radiation pollution and electromagnetic (EM) interference issues have aroused wide concern in the major field of mobile communication and military application (Ref 1-3). As a useful shielding material, radar absorbing material (RAM) can restrain electromagnetic interference to a certain extent. For strategic and commercial applications, RAM requires wide bandwidth, significant absorption, lightweight, thin thickness, high cost-effectiveness and easy manufacturing (Ref 4). However, all abovementioned requirements cannot be met by using traditional absorbing materials.

Graphene nanosheets (GNSs), a new class of two-dimensional carbon nanostructure, have attracted tremendous attention due to their excellent properties, such as the large specific surface area, high Young's modulus, excellent thermal transport, electrical and mechanical properties (Ref 5-9). These properties make graphene become a promising candidate as a RAM absorber. However, the low impedance matching of GNS caused by the high carrier mobility directly reflect the electromagnetic wave (Ref 10-12). Up to now, many researchers have studied the microwave absorption performance of GNS coupling with other materials. Qing et al. (Ref 13) fabricated GNSs/Al_2O_3 by hot pressing sintering to obtain the minimum reflection loss (RL_{min}) values with −24 dB and reflection loss (RL) ≤ -10 dB bandwidth from 9.1-10.7 GHz. Zhang et al. (Ref 14) investigated the microwave absorption properties of graphene-CdS nanocomposite, and the RL ≤ -10 dB bandwidth in the frequency range of 5.2–18 GHz when adjusting the thicknesses from 2 to 5 mm. It concluded from

Published online: 18 June 2021

the above-mentioned research literature that good electromagnetic absorption properties with thin-thickness and wide absorption frequency band could be realized by reasonable construction of graphene-based nanocomposites.

Zinc oxide (ZnO) possesses many superior and unique electrical properties, which can be used as an absorbent to enhance the conductivity of composite materials (Ref 15-17). Hu et al. (Ref 18) prepared the flower-shaped ZnO, and the RL_{min} values were −21.85 dB with a thickness of 3.0 mm. However, the absorption efficiency of ZnO is still limited ascribe to its single attenuation mechanism (Ref 19). Currently, most studies combine graphene with ZnO, and found that ZnO could enhance the impedance matching of graphene and serve as capacitance-like to improve the microwave absorption performance (Ref 19, 20). Han et al. (Ref 21) reported that the graphene/ZnO composite material showed stronger microwave absorption properties in X band compared to pure ZnO nanostructures.

In recent years, air plasma spraying (APS) is becoming a promising technique for microwave absorbing application, owing to the high achievable deposition efficiency and simple operational approach, cost-effectiveness and very specific coating properties, (Ref 22-24). Su et al. (Ref 25) prepared Ti_3SiC_2/cordierite coatings by APS, the RL_{min} values were -33.4 dB and the absorption bandwidth (≤ -5 dB) covered the X-band with a thickness of 1.8 mm. Qing et al. (Ref 26) fabricated FeSiAl/flake graphite-filled Al_2O_3 composite coating by APS, and the RL values less than −7 dB can be obtained in the whole Ku-band with the sample thickness just 0.8 mm. However, until now, the dielectric and microwave absorption properties of the plasma-sprayed doped GNS coatings have rarely been studied. The coatings with GNS can generate interfacial polarization and providing more dielectric loss, which is expected to improve the microwave absorption. Al_2O_3 has excellent mechanical properties such as high strength, high hardness, low density and high-temperature corrosion resistance, which is widely used as the matrix of composite coatings (Ref 27).

Herein, GNS and ZnO powders used as the conductive filler were introduced into Al_2O_3 matrix for fabricating the microwave absorbers. The GNSs/ZnO/Al_2O_3 coatings with different GNS content and constant ratio of ZnO and Al_2O_3 were prepared by APS technology. Their dielectric properties and microwave absorption properties were investigated with the frequency range of 8.2-12.4 GHz (X-band). The effects of GNS content, ZnO and frequency on the electromagnetic properties of GNSs/ZnO/Al_2O_3 composite coatings were studied.

Experimental

Preparation of Spray-Dried Powders

The GNSs were obtained by the exfoliation of graphite with typical thickness and lateral dimensions of about 2-10 nm and 5-15 μm, respectively. The commercially available ZnO nano-powder with an average particle size of 50 nm and Al_2O_3 powders with an average particle size of 0.6-0.8 μm were used as the raw powder.

GNSs were ultrasonicated for 1h in alcohol with a concentration of about 1 mg/ml, and ZnO, Al_2O_3 were added into the GNS suspension followed by a homogenizer (BME100LX, Shanghai Weiguang Machinery Manufacturing Co., Ltd, China) with a speed of 4500 r/min for another 4h. Then, the powders were fully dried in an oven at 50°C. The content of ZnO was kept at 20 wt.%. The content of GNS was 0, 5.0, 10.0 and 15.0 wt.% in the Al_2O_3 matrix and the corresponding samples were designated as GN0, GN5, GN10 and GN15 for simplicity.

Spray-dried was selected for mixing, agglomerating the spray powders with different GNS content. The ground powder was mixed with distilled water according to the ratio of powder to water = 4:6, and then added polyvinyl alcohol (PVA) solution with powder mass of 1 wt.% to stir 0.5 h. The spray-dried parameters are given in Table 1. The obtained porous spherical nanostructured agglomerates are with a diameter of 70 ± 15 μm.

Preparation of the Coatings

Prior to plasma spray, 45# substates (100 mm×15 mm×5 mm) were blasted using Al_2O_3 particles with an average size of ~1mm and followed by being cleaned with acetone. These spherical spray-dried agglomerates were plasma-sprayed using SG 100 gun (Praxair Surface Technology, Danbury, CT) on 45# substate, and the details of operating spraying parameters are listed in Table 2. When the coating thickness reached 2.5 mm, the coating peeled off from the 45# steel due to the thermal stress between the coating and the substrate. Then, the samples were processed into a rectangle (10.16 mm × 22.86 mm) with a

Table 1 Spray-dried parameters

Spray-dried parameters	Value
Entry air temperature, °C	290-330
Exit air temperature, °C	120-130
Nozzle rotation speed, r/s	32
Slurry flow rates, rpm	28

Table 2 APS deposition parameters

APS deposition parameters	Value
Plasma current, A	800
Plasma voltage, V	40
Primary gas, Ar flow rate, slpm	37
Secondary gas, He flow rate, slpm	39
Power carrier gas, Ar flow rate, slpm	9
Powder feed rate, r/min	2
Plasma distance, mm	70

thickness of 2 mm, and the complex dielectric properties of 8.2 $\sim$ 12.4 GHz were measured.

Characterizations of Powders and Coatings

The phase compositions of spray-dried powders and coatings were identified by Ultima IV multi-function x-ray diffractometer (XRD) at 40 KV, 40 mA. Microstructure observations of the composite powders and coatings were performed using a scanning electron microscope (SEM, Hitachi S-4700, Japan). The Raman spectroscopy was conducted to detect the presence of GNS (LabRam HR800, HORIBA, France) with an Argon ion laser of wavelength 633 nm and an acquisition time of 10 s. The complex permittivity was determined by the Agilent Technologies N5230C PNA network analyzer with the wave guide method in the frequency range of 8.2-12.4 GHz. The Vickers hardness (HV) test was performed with an applied load of 2 N with dell time 10 s following the standard specification for HXD-1000TMC at least 10 times. The density and porosity of the coating were measured by the Archimedean principle. The porosity of each coating was calculated as follows:

$$\text{Porosity}(\%) = 1 - \frac{\text{Actual density}}{\text{Theoretical density}} \times 100\% \qquad \text{(Eq 1)}$$

Results and Discussion

The overall process of coating preparation is shown in Fig. 1. Although the thickness of the as-received GNS according to the manufacturer's specification is 2-10nm, the intrinsic van der Waals among the GNSs can result in a significant agglomeration as seen in the inset part of Fig. 1. The high shear force, which was produced in the shear gap between the rotor and the stator of the homogenizer mixer, could homogeneously disperse the agglomerated GNSs. Meanwhile, the dispersed GNSs are interpenetrated between Al_2O_3 and ZnO particles, which would inhibit the reagglomeration of GNSs. The raw powders cannot be directly sprayed using the regular powder feeders due to tiny particles usually clog the hoses. Herein, the spray-dried was employed to obtain microsized agglomerates with good flowability for plasma spraying. The powder is melt into a droplet by using plasma spraying, which gives the particles high-speed movement, so that the coating is fabricated by one layer of one layer accumulated on the substrate.

The SEM image of GNSs/ZnO/Al_2O_3 composite powder after spray-dried in Fig. 2(a) clearly displays that the powder is produced in a spherical shape to ensure sufficient fluidity for plasma spraying. The particle diameter on 3-5 SEM images were calculated to obtain the average diameter size of these composite powders is about 70 $\pm$ 15 μm. One of the important tasks of GNSs reinforced coatings is to obtain homogeneous dispersion of GNSs, because GNSs will easy agglomerate due to van der Waals force. Figure 2(b) clearly shows that GNSs are homogeneously dispersed in the composites after dispersing by homogenizer, which will form more interfacial polarization in the material and improve the microwave absorption properties. Furthermore, Fig. 2(c) shows that the GNS has few layers, indicating that GNS has changed from the original multi-layer structure to a single-layer or a few layers structure after dispersion.

Figure 3 shows the typical fracture surface of GNSs/ZnO/Al_2O_3 composite coatings. During the plasma spraying process, the ZnO-Al_2O_3 particles could be melted to form a droplet with the dispersed GNSs. After cooling, the GNS will be trapped by solidified ZnO-Al_2O_3 in Fig. 3(a), which not only forms a supporting framework structure, but also improves the cohesion strength of the coating. Meanwhile, the reduced resistivity of the coatings is conducive to the matching of the characteristic impedance of the coating and the free impedance of the space, which make the electromagnetic wave fully absorbed into the coatings. Figure 3(b) shows that GNSs are uniformly dispersed in the composite coatings and solidified in the morphology of the composite coatings, indicating that there is good interface compatibility between GNS and coatings. During the plasma spraying process, the GNS structure remains and the sheet structure is clearly visible. The further increase in GNS content leads to the stacking of GNS, and the stacked GNS will increase the porosity of the coating and easily form a three-dimensional conductive path, which is shown in Fig. 3(c).

Since the phase composition of these components may change during plasma spraying process. XRD was employed to analyze the phase of the spray-dried and plasma-sprayed composites. Figure 4 shows the XRD patterns of the spray-dried GNSs/ZnO/Al_2O_3 composite powders and coatings. As shown in Fig. 4(a), the spray-dried powders are mainly composed of ZnO and Al_2O_3,

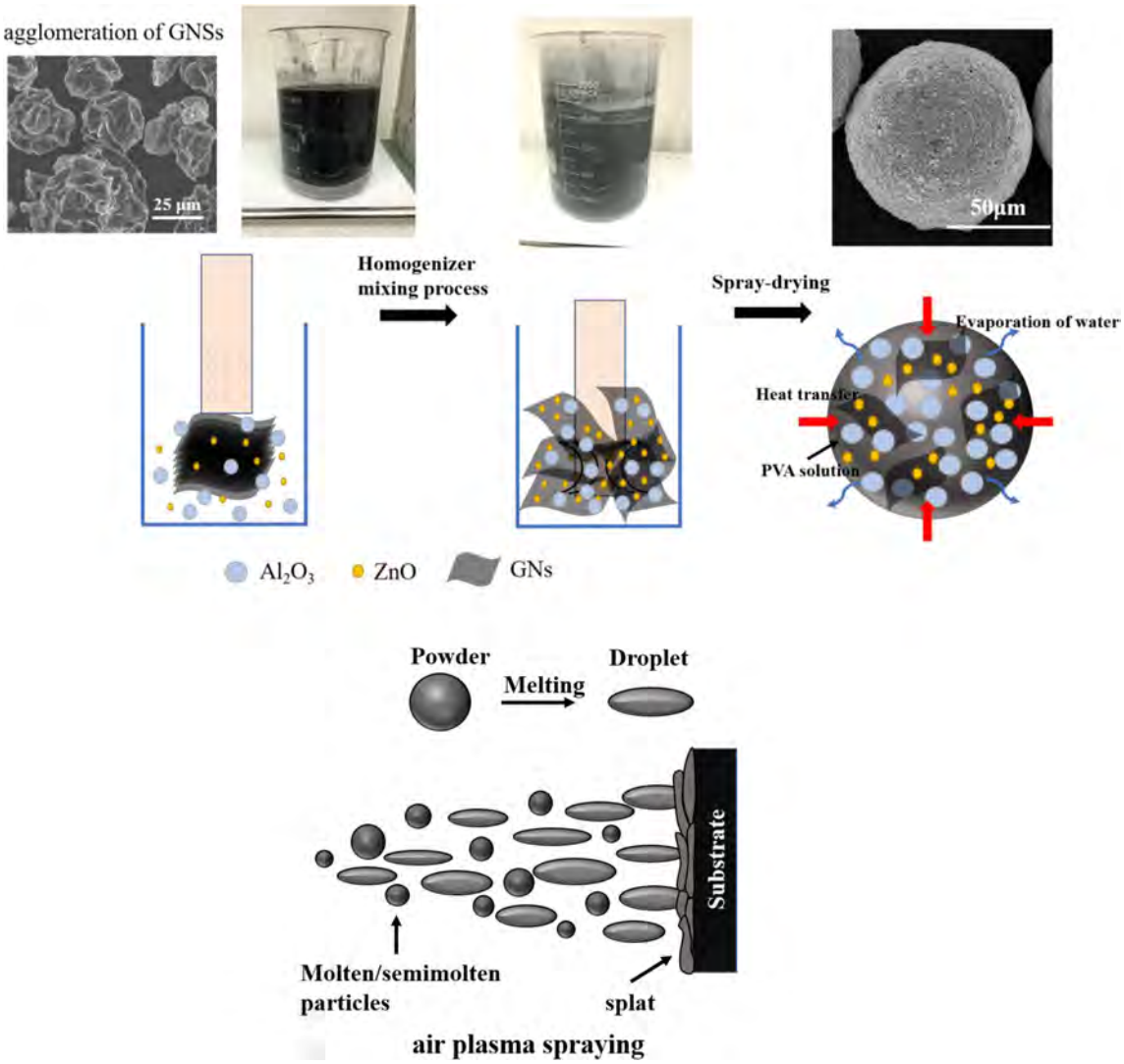

Fig. 1 Schematic illustration of GNSs/ZnO/Al_2O_3 composite coating fabrication process

and there is no detectable other phase indicating that there has not been any significant reaction. The diffraction peaks at $2\theta = 26.3°$ on the patterns of the composites correspond to carbon and increase with the increase in GNS content. Figure 4(b) shows that all coatings contain α-Al_2O_3 and γ-Al_2O_3 phases, γ-Al_2O_3 is the predominant phase compared to the peak intensity of α-Al_2O_3, which is owing to the α-Al_2O_3 will inevitably form γ-Al_2O_3 in the process of plasma spraying due to the rapid solidification of the droplet (Ref 28). The presence of α-Al_2O_3 is due to incomplete melting or partial melting of particles during the spraying process. However, Al_2O_3, a matrix phase, has extremely low dielectric loss and conductivity (Ref 29, 30). It has the property of wave transmission and hardly affects the microwave absorption. In addition, $ZnAl_2O_4$ phase is found in the coating, owing to the solid phase reaction of ZnO and Al_2O_3 above 600 °C (Ref 15).

Figure 5 shows Raman spectra of pure GNS and sample GN5 powder and coating. The Raman peak of GNS at 1348 cm^{-1} is assigned to the D-band, which is ascribed to the presence of local defects and disorder, and the peak at 1583 cm^{-1} called as G-band originates from the in-plane vibration of sp^2 carbon atoms (Ref 19). It should be noted that the G peak in the pure GNS is quite high intensity, because the C-C in the GNS is integrated. For sample GN5 due to the shearing force produced by mixer, the defects of GNS increase leading to the G-band is reduced. In generally, it often uses the ratio of the intensity of D and G band (I_D/I_G) to evaluate the disorder and defect degree of GNS. The I_D/I_G value of the GN5 powder and coating is 0.95 and 1.01, respectively, revealing an increased degree of disorder and defect in the composites compared with the value 0.37 of pure GNS. The increase of disorder is due to the

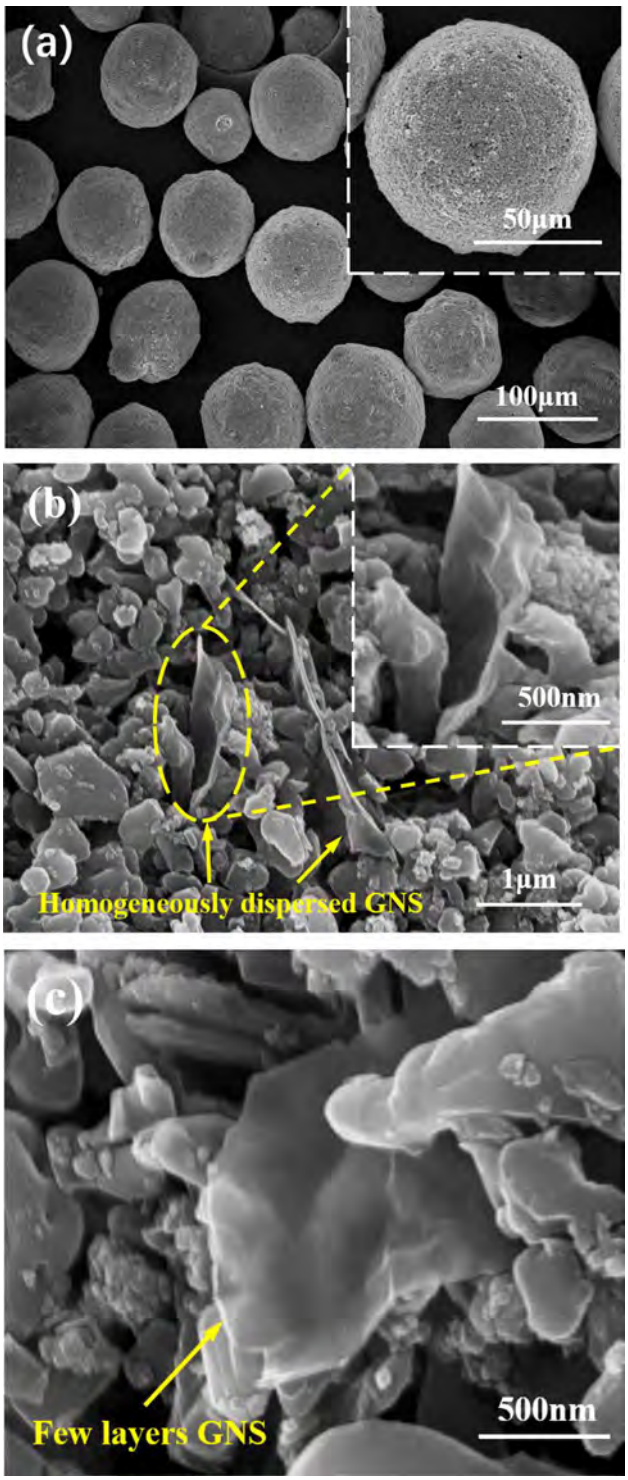

Fig. 2 SEM images of (a) spray-dried agglomerated GNSs/ZnO/Al_2O_3 composite powders, the inset window showing high magnification of the spray-dried powders, (b) GNSs dispersed in the composite powders, and the inset shows high magnification GNS, and (c) GNS is homogeneously dispersed on the surface with few layers

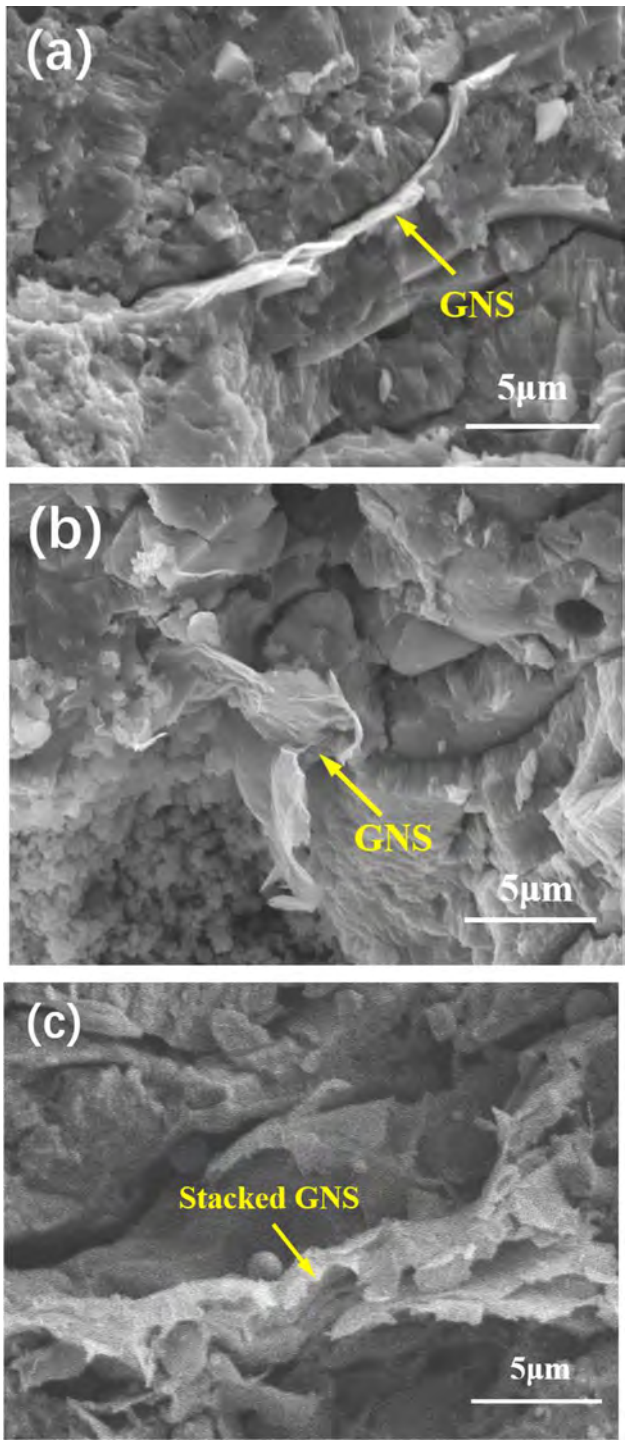

Fig. 3 Typical fracture surface of SEM images of (a) GNS is trapped by molten ZnO-Al_2O_3, (b) GNSs are uniformly dispersed in the coating and solidified in the morphology of the composite coating in sample GN5, and (c) GNS agglomeration in sample GN15

interpenetration and adhesion of ZnO and Al_2O_3 on the surface of GNS, which disrupts the original order of GNS. More defects can induce defect polarization relaxation with the capacity of promoting the microwave

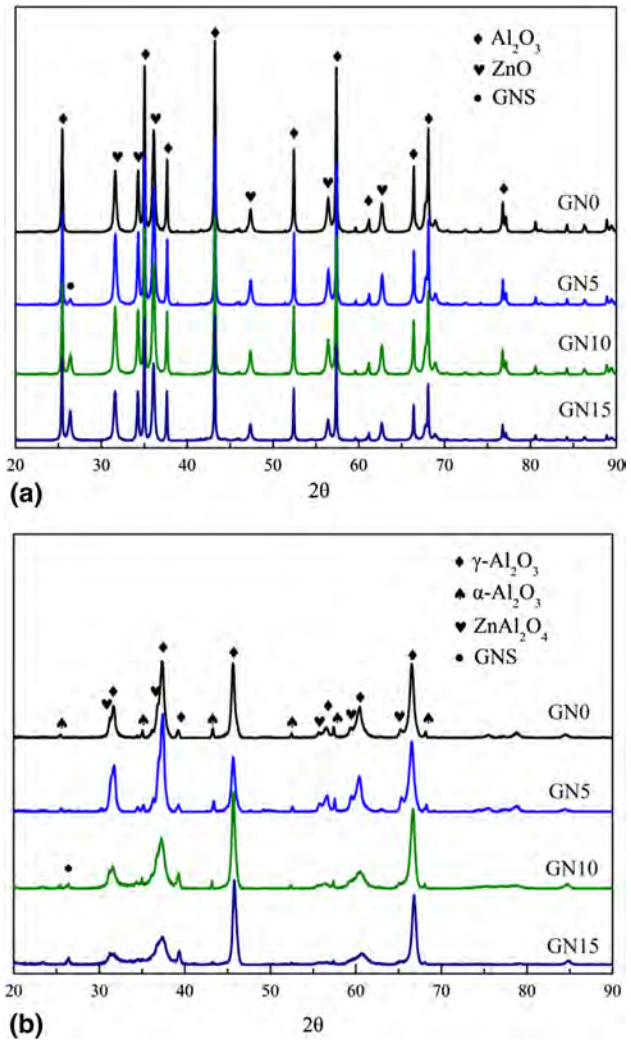

Fig. 4 XRD results for (a) the spray-dried powders and (b) coatings of the GNSs/ZnO/Al_2O_3 composites

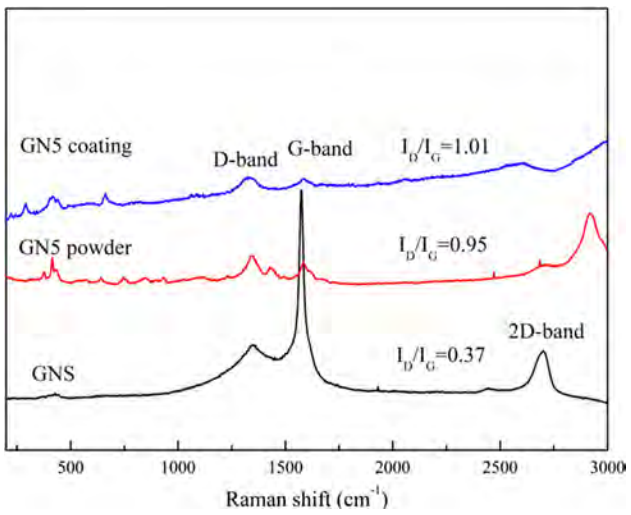

Fig. 5 Raman spectra of GNS and sample GN5 composite powder and coating

absorption under the varying electromagnetic field (Ref 31). Meanwhile, the disordered structure forms the defect polarization center, which can promote the attenuation of incident electromagnetic waves (Ref 4).

Table 3 shows the variation of porosity and hardness of the coatings with different content of GNS. The porosity decreased from 10.7 to 9.3% with introduced GNS. The decrease in porosity due to the fact that GNS can better fill the unmelted or partially melted pores in the coating. However, the porosity increases from 9.3 to 9.9% with the GNS content increases from 5 to 15 wt.%. Combined with the analysis of the cross-section morphology, the reason for the increase in porosity is the partial agglomeration of GNS. The hardness of the coating increased from 914.2 to 1057.3 $HV_{0.2}$ and such an improvement is attributed to the addition of GNS. The increase of hardness is due to the decrease of the porosity of the coating, and GNS with high Young's modulus and large specific area are well-dispersed in the composites, reinforcing and helping the transfer of the load from the composite coatings. However, the excessive content of GNSs tend to agglomerate to form clusters in virtue of strong van der Waals interactions, which to form more porosities and reduce the mechanical properties (Ref 32).

The real part (ε') and imaginary part (ε'') are shown in Fig. 6(a) and (b), respectively. It can be observed that both the values of ε' and ε'' of the GNSs/ZnO/Al_2O_3 coating increases with the increase in GNS content in the whole measured frequency region. The value of ε' significantly increase from 7.0 to 12.4, and the value of ε'' increase from 0.1 to 1.1. The dielectric loss mechanism of GNSs/ZnO/Al_2O_3 composite coating is mainly caused by the polarizability and dielectric loss of a material which mainly depend on interfacial polarization and dipolar polarization (Ref 8). Therefore, the interfaces and dipoles in the samples increase as the GNS percentage enhances resulting to the growth of ε' and ε''.

The value of ε' represents the storage capacity of electromagnetic wave energy and mainly depends on the polarization process of materials (Ref 33). Due to the uniform dispersion of GNS in the composites, the interfacial polarization generated at the heterointerfaces between the GNS and other materials when such coatings suffer from an applied field. With the increase in GNS content, the increase of conductivity and interfacial polarization leads to the increase of the value of ε' of the coating (Ref 13). In addition, due to the excellent semiconductor properties of ZnO, capacitance-like structures will be formed in the layer-by-layer stacked periodic structures. The formation of a large number of capacitance-like structures will enhance the polarization mechanism (Ref 34). Furthermore, due to the atomic migration and rearrangement during the formation of $ZnAl_2O_4$, oxygen vacancy defects

Table 3 Porosity and hardness of the coating with different content of GNS

	GN0	GN5	GN10	GN15
Porosity, %	10.7 ± 0.9	9.3 ± 0.7	9.7 ± 0.8	9.9 ± 0.8
Hardness ($HV_{0.2}$)	914.2 ± 38.8	1046.3 ± 47.8	1001.4 ± 42.2	1057.3 ± 48.5

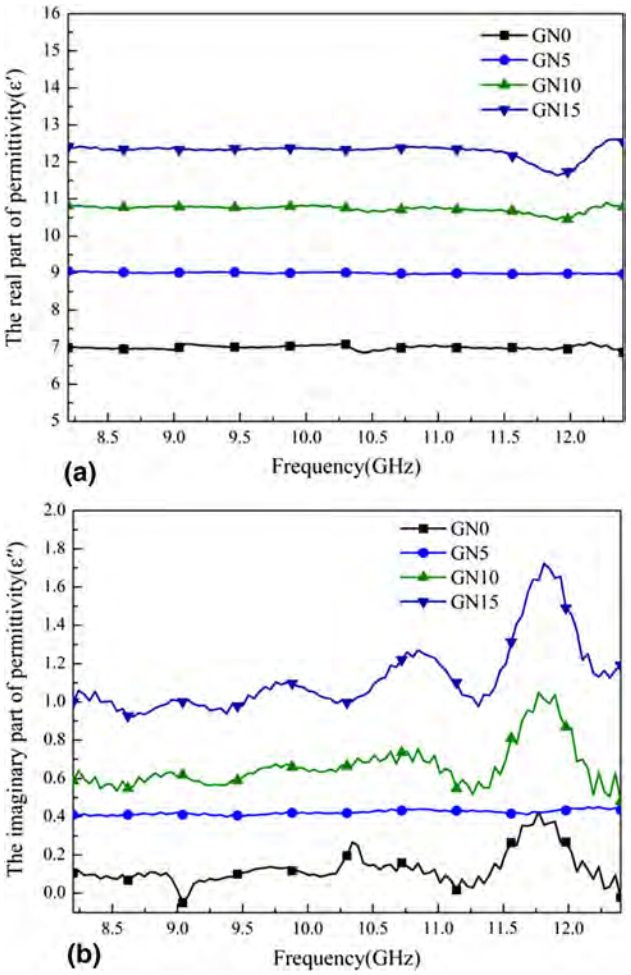

Fig. 6 The (a) real and (b) imaginary parts of complex permittivity of GNSs/ZnO/Al_2O_3 composite coatings with different GNS content

easily increase the dipole polarization position (Ref 15). From these points of view, the higher value of ε' can be obtained with an increase in GNS content and ZnO.

The value of ε'' represents the loss ability of EM wave energy, which mainly depends on relaxation phenomenon and electrical conductivity (Ref 35). ε'' can be expressed by the equation:

$$\varepsilon'' = \varepsilon''_{\text{relax}} + \sigma/\omega\varepsilon_0 \quad \text{(Eq 2)}$$

where ε''_{relax} is the electron relaxation process in this case, σ is the electrical conductivity, ε_0 is the dielectric constant in a vacuum, and ω is the angular frequency (Ref 13). According to the above formula, with the increase in GNS content, $\varepsilon''_{\text{relax}}$ and σ will be enhanced, resulting in an increase in the value of ε''. The composite coatings with increasing GNS content have more interfacial electric dipole polarization, which requires longer relaxation time in the test frequency range (Ref 6). Therefore, higher values of ε' and ε'' can be obtained under the higher electrical conductivity of such composite coating. Furthermore, under an alternating EM field, the carriers generated by defects in ZnO crystal will migrate back and forth, forming relaxation polarization and loss respectively, which also makes the ε'' of the coating increase (Ref 36).

According to the above electromagnetic parameters and transmission line theory, the value of reflection loss (RL) of single-layer GNSs/ZnO/Al_2O_3 coating with different thickness can be calculated as following (Ref 37, 38):

$$\text{RL(dB)} = 20\log_{10}\left|\frac{(Z_{\text{in}} - Z_0)}{(Z_{\text{in}} + Z_0)}\right| \quad \text{(Eq 3)}$$

where Z_0 is the characteristic impedance of free space. Z_{in} is the input characteristic impedance at the absorber and free space interface, which can be expressed as:

$$Z_{\text{in}} = \left(\frac{\mu_r}{\varepsilon_r}\right)^{1/2}\tanh\left[j\left(\frac{2\pi fd}{c}\right)(\mu\varepsilon_r)^{1/2}\right] \quad \text{(Eq 4)}$$

where μ_r and ε_r are the relative permeability and permittivity of the absorber, respectively; f is the frequency of the electromagnetic wave; d is the thickness of the absorber; c is the velocity of light in free space.

The RL of GNSs/ZnO/Al_2O_3 composite coatings is calculated based on the complex permittivity in the X-band with optimum thicknesses, as shown in Fig. 7(a). When the thickness is 2.0 mm, the RL of the coatings GN0 and GN5 cannot reach −5 dB (larger than 68.4% absorption), indicating extremely poor microwave absorption properties. It is mainly ascribed to the poor ε'' values due to the low content of absorber and inferior microwave attenuation characteristics. When the GNS content increases to 10 wt.%, the reflectivity of the GN10 coating reaches the minimum value of −9 dB (87.4% absorption) at 11.6 GHz. As the GNS content increases to 15 wt.%, the GN15 coating exhibits excellent microwave absorption properties. The minimum value of RL (RL_{min}) is -45 dB (large than 99% absorption) at 11.5 GHz and RL ≤ −10 dB (90% absorption) bandwidth in the frequency range of 11.2-12.0 GHz when the thickness is 1.82 mm. GNSs filled ZnO/Al_2O_3 composite coating satisfy the requirements of impedance matching, possess strong electromagnetic absorption properties and broader absorption bandwidth.

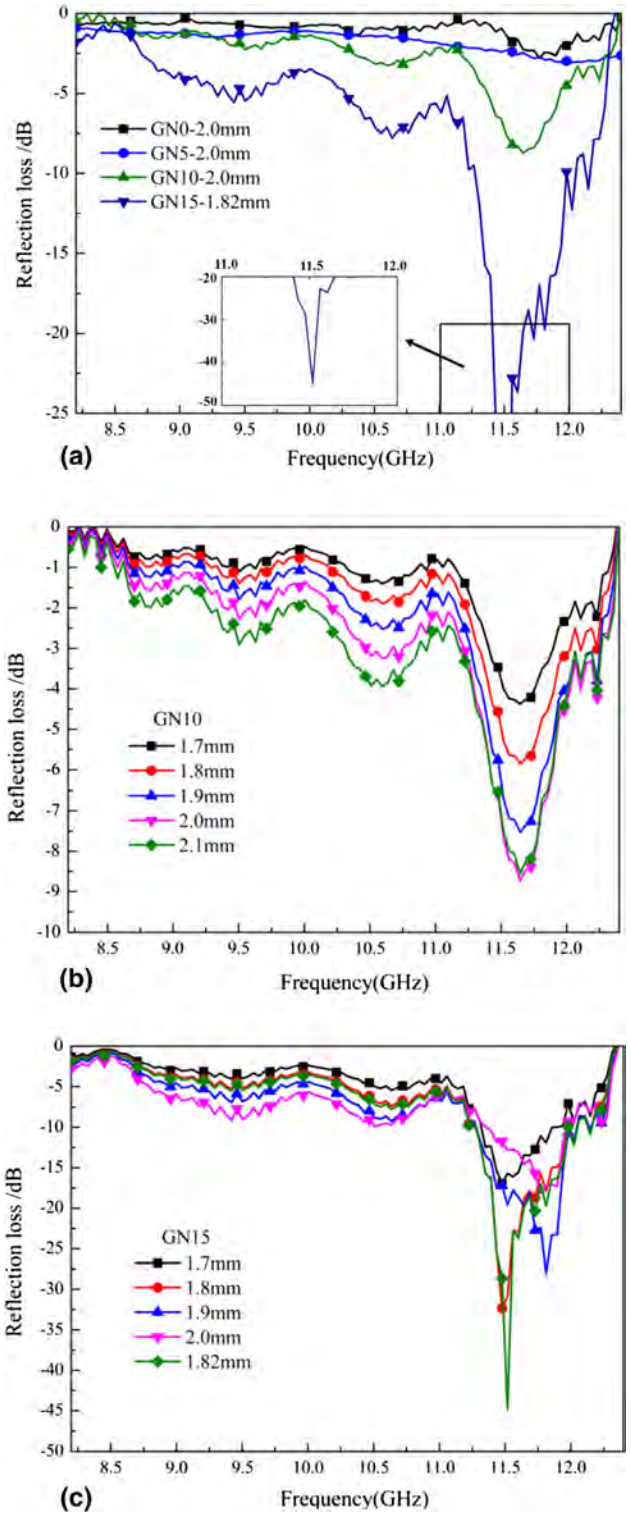

Fig. 7 (a) The RL of the GNSs/ZnO/Al_2O_3 composite coatings with different GNS content under optimum thicknesses to obtain wideband absorption in the X-band. Reflection loss of GNSs/ZnO/Al_2O_3 coatings with different thickness for GNS content 10 wt.% (b) and 15 wt.% (c), respectively

Figure 7(b) and (c) shows the calculated RL of sample GN10 and GN15 with the different thicknesses. It can be found that the value of RL increased with the increase of coating thickness in the whole frequency range. When the thickness is up to 2.1 mm, the value of RL of the sample GN10 reaches the minimum −9 dB and the RL $\leq$ −2 dB broadband in the frequency range of 9.3-12.2 GHz. As for the GN15, when the thickness increases to 2mm, the maximum reflectivity decreases, but the bandwidth increases. The RL_{min} is −18 dB at 11.8 GHz and the RL $\leq$ −5 dB broadband in the frequency range of 8.8-12.3 GHz with the thickness of 2.0 mm. The microwave absorption of the GN15 sample is much higher than that of the GN10 sample, which is ascribed to the increased coating interfacial polarization and the deflection of dipole with the increase of GNS content.

We compare the performance of the GN15 sample with several coatings in previous reports, including various composites, as shown in Table 4. The GN15 exhibits a better minimum RL value, equivalent absorbing bandwidth and thinner thickness. It demonstrates the great effect of dielectric regulation on the microwave absorption properties using the GNS and ZnO introduced in coatings.

In view of the above discussion, the mechanism for excellent microwave absorption properties of GNSs/ZnO/Al_2O_3 composite coatings was discussed as follows. Considering that the mechanism of microwave absorption mainly comes from the medium, so it is closely related to the conductivity of the medium. The strong attenuation capability due to the dielectric loss and conduction loss ensured the more EM energy dissipation. With introduced GNS and ZnO and homogeneously dispersed, the coating possessed high conductivity and form more interfacial polarization, which can provide excellent dielectric loss (Ref 4). Based on Raman results the I_D:I_G ratio increases, and means the defects of GNS and the number of dipoles increase, which will convert electromagnetic energy to heat energy due to the relaxation loss (Ref 39). In addition, due to EM wave can only be absorbed by incident into the coating, the impedance matching with free space should also be considered. After plasma spray, GNS is trapped by molten ZnO-Al_2O_3 and embedded in the coatings, which reduces the resistivity of the coating to improve impedance matching. Furthermore, the impedance matching of GNS can be further improved by the uniformly dispersed ZnO nanocrystals, leading to an increase in microwave absorption (Ref 8).

Table 4 Summary of microwave absorption properties for the coatings in previous works

Materials	Thickness, mm	−10dB bandwidth , GHz	RL_{min}, dB	f/GHz	References
Cr/Al_2O_3	1.5	0	−9.3	12.3	(Ref 28)
TiO_2/Al_2O_3	3	0.5	−10.5	9.4	(Ref 40)
Fe/Al_2O_3	1.7	1.2	−15	9	(Ref 41)
NiCrAlY/ Al_2O_3	2	1.3	−15.7	8.9	(Ref 42)
Ti_3SiC_2/NASICON	1.4	0.6	−12.4	9.63	(Ref 43)
SiC/SiO_2	2.3	0.3	−11.6	7.1	(Ref 44)
Carbon fibers/glass	2.4	2.1	−29.9	9.2	(Ref 45)
GN15	1.82	0.8	−45	11.5	This work

Conclusions

In this study, GNSs/ZnO/Al_2O_3 composite coatings were prepared by air plasma spraying technique. The SEM results show that the GNS is homogeneously dispersed in the composites, which will form more interfacial polarization and improve the microwave absorption properties. XRD showed that the main components of the powder were ZnO and Al_2O_3 phase, and the main components of the coating were α-Al_2O_3, γ- Al_2O_3 and $ZnAl_2O_4$ phase. Raman spectra show the I_D /I_G values of the powder and coating are 0.95 and 1.01, respectively. The porosity decreased from 10.7% to 9.9% and the hardness of the coating reaches 1057.3 $HV_{0.2}$ for sample GN15. The effect of GNS content on dielectric behavior and microwave absorption properties of GNSs/ZnO/Al_2O_3 coatings were investigated in the X-band. The results indicated that both the dielectric constant and reflection loss of the coatings increased with increase in GNS content. The ε′ and ε″ of the dielectric constant of the coatings increase from 7.0 to 12.4 and 0.1 to 1.1, respectively. As the GNS content increases to 15 wt.%, the coating exhibits excellent microwave absorption properties. The RL_{min} is −45 dB (large than 99% absorption) at 11.5 GHz and RL ≤ −10 dB (90% absorption) bandwidth in the frequency range of 11.2-12.0 GHz when the thickness is 1.82 mm. By introducing GNS and ZnO, the conductivity, interfacial polarization and impedance matching of the coating are increased, which improve the microwave absorbing performance. The prepared coatings have microwave absorption properties as well as excellent mechanical properties.

Acknowledgments This research work was financially supported by National Natural Science Foundation of China (Grant Numbers: 51501121, 51475315, 51775360, 51701134, 52071124), National Key R&D Program of China (2017YFB1103601), and NSAF (Grant No. U2030102) for financial support.

References

1. Z.-N. Yang, F. Luo, W.-C. Zhou, D.-M. Zhu and Z.-B. Huang, Design of a Broadband Electromagnetic Absorbers Based on TiO_2/Al_2O_3 Ceramic Coatings With Metamaterial Surfaces, *J. Alloy. Compd.*, 2016, **687**, p 384–388.
2. Z.-N. Yang, F. Luo, J.-S. Xu, W.-C. Zhou and D.-M. Zhu, Dielectric and Microwave Absorption Properties of $LaSrMnO_3$/Al_2O_3 Ceramic Coatings Fabricated By Atmospheric Plasma Spraying, *J. Alloy. Compd.*, 2016, **662**, p 607–611.
3. Y.-C. Qing, J.-B. Su, Q.-L. Wen, F. Luo, D.-M. Zhu and W.-C. Zhou, Enhanced Dielectric and Electromagnetic Interference Shielding Properties of FeSiAl/Al_2O_3 Ceramics by Plasma Spraying, *J. ALLOY. COMPD.*, 2015, **651**, p 259–265.
4. S.K. Singh, M.J. Akhtar and K.K. Kar, Impact of Al_2O_3, TiO_2, ZnO and $BaTiO_3$ on the microwave absorption properties of exfoliated graphite/epoxy composites at X-band frequencies, *Compos. Part B: Eng.*, 2019, **167**, p 135–146.
5. L. Kong, X.-W. Yin, M.-K. Han, L.-T. Zhang and L.-F. Cheng, Carbon Nanotubes Modified with ZnO Nanoparticles: High-Efficiency Electromagnetic Wave Absorption at High-Temperatures, *CERAM. INT.*, 2015, **41**(3B), p 4906–4915.
6. Y.-C. Qing, Q.-L. Wen, F. Luo, W.-C. Zhou and D.-M. Zhu, Graphene Nanosheets/$BaTiO_3$ Ceramics as Highly Efficient Electromagnetic Interference Shielding Materials in the X-Band, *J. Mater. Chem. C.*, 2016, **4**(2), p 371–375.
7. C.-P. Mu, X. Du, A. Nie, B.-C. Wang, F.-S. Wen, J.-Y. Xiang, K. Zhai and Z.-Y. Liu, Microwave Absorption Properties of Heterostructure Composites of Two Dimensional Layered Magnetic Materials and Graphene Nanosheets, *Appl. Phys. Lett.*, 2019, **115**, p 0431034.
8. W. Feng, Y.-M. Wang, J.-C. Chen, L. Wang, L.-X. Guo, J.-H. Ouyang, D.-C. Jia and Y. Zhou, Reduced Graphene Oxide Decorated with In-Situ Growing ZnO Nanocrystals: Facile Synthesis and Enhanced Microwave Absorption Properties, *Carbon*, 2016, **108**, p 52–60.
9. Y. Song, Y. Chen, W.W. Liu, W.L. Li, Y.G. Wang, D. Zhao and X.B. Liu, Microscopic Mechanical Properties of Titanium Composites Containing Multi-Layer Graphene Nanofillers, *Mater. Design.*, 2016, **109**, p 256–263.
10. H.-F. Li, J. Wang, Y.-H. Huang, X.-Q. Yan, J.-J. Qi, J. Liu and Y. Zhang, Microwave Absorption Properties of Carbon Nanotubes and Tetrapod-Shaped ZnO Nanostructures Composites, *Mater. Sci. Eng. B-Adv.*, 2010, **175**(1), p 81–85.
11. Y.-F. Zhu, Q.-Q. Ni and Y.-Q. Fu, One-Dimensional Barium Titanate Coated Multi-Walled Carbon Nanotube Heterostructures: Synthesis and Electromagnetic Absorption Properties, *RSC. Adv.*, 2015, **5**(5), p 3748–3756.
12. X. Gui, W. Ye, J. Wei, K. Wang, R. Lv, H. Zhu, F. Kang, J. Gu and D. Wu, Optimization of Electromagnetic Matching of Fe-

Filled Carbon Nanotubes/Ferrite Composites for Microwave Absorption, *J. Phys. D: Appl. Phys.*, 2009, **42**(7), p 075002.
13. Y.-C. Qing, Q.-L. Wen, F. Luo and W.-C. Zhou, Temperature Dependence of the Electromagnetic Properties of Graphene Nanosheet Reinforced Alumina Ceramics in the X-band, *J. Mater. Chem C.*, 2016, **4**(22), p 4853–4862.
14. D.-D. Zhang, D.-L. Zhao, J.-M. Zhang and L.-Z. Bai, Microwave Absorbing Property and Complex Permittivity and Permeability of Graphene-CdS Nanocomposite, *J. Alloy. Compd.*, 2014, **589**, p 378–383.
15. P. Wei, D. Zhu, S. Huang, W. Zhou and F. Luo, Effects of the Annealing Temperature And Atmosphere on the Microstructures and Dielectric Properties of ZnO/Al_2O_3 composite coatings, *Appl. Surf. Sci.*, 2013, **285**, p 577–582.
16. N. Yang, J. Zeng, J. Xue, L.-K. Zeng and Y. Zhao, Strong Absorption and Wide-Frequency Microwave Absorption Properties of the Nanostructure Zinc Oxide/Zinc/Carbon Fiber Multilayer Composites, *J. Alloy. Compd.*, 2018, **735**, p 2212–2218.
17. W.-D. Zhang, Y. Zheng, X. Zhang, Q. Zhu, L.-L. Tian, H.-J. Wu, H.-X. Yan and S.-H. Qi, Structure-Microwave Absorption Performance Correlations of GNPs/ZnO Nanocomposite Absorber: Synthesis, Characteration and Mechanism Investigation, *Ceram. Int.*, 2019, **45**(10), p 13376–13384.
18. Q. Hu, G.-X. Tong, W.-H. Wu, F.-T. Liu, H.-S. Qian and D.-Y. Hong, Selective Preparation and Enhanced Microwave Electromagnetic Characteristics of Polymorphous ZnO Architectures Made from a Facile One-Step Ethanediamine-Assisted Hydrothermal Approach, *CrystEngComm*, 2013, **15**(7), p 1314–1323.
19. W. Feng, Y.-M. Wang, J.-W. Chen, L.-X. Guo, J.-H. Ouyang, D.-C. Jia and Y. Zhou, yMicrowave Absorbing Property Optimization of Starlike ZnO/Reduced Graphene Oxide Doped by ZnO Nanocrystal Composites, *Phys. Chem. Chem Phys.*, 2017, **19**(22), p 14596–14605.
20. S. Yang, X. Guo, P. Chen, D.-W. Xu, H.-F. Qiu and X.-Y. Zhu, Two-step synthesis of self-assembled 3D graphene/shuttle-shaped zinc oxide (ZnO) nanocomposites for high-performance microwave absorption, *J. ALLOY. COMPD.*, 2019, **797**, p 1310–1319.
21. M.-K. Han, X.-W. Yin, L. Kong, M. Li, W.-Y. Duan, L.-T. Zhang and L.-F. Cheng, Graphene-Wrapped ZnO Hollow Spheres with Enhanced Electromagnetic Wave Absorption Properties, *J. Mater. Chem A.*, 2014, **2**(39), p 16403–16409.
22. X.-L. Lu, S. Bhusal, G.-Y. He, D. Zhao, C. Zhang, A. Agarwal and Y. Chen, Efficacy of Graphene Nanoplatelets on Splat Morphology And Microstructure of Plasma Sprayed Alumina Coatings, *Surf. Coat. Technol.*, 2019, **366**, p 54–61.
23. J.-B. Su, W.-C. Zhou, Y. Liu, Y.-C. Qing, F. Luo and D.-M. Zhu, Effect of Carbon Black on Dielectric and Microwave Absorption Properties of Carbon Black/Cordierite Plasma-Sprayed Coatings, *J. Therm. Spray Technol.*, 2015, **24**(5), p 826–835.
24. H.-F. Lou, J.-J. Wang, Y.-S. Hou, M. He and Z.-N. Zhao, High-Frequency Absorption Properties of Three Kinds of Hollow Multiphase Ceramic Microspheres, *J. Therm. Spray Technol.*, 2014, **23**(3), p 492–501.
25. J.-B. Su, W.-C. Zhou, Y. Liu, Y.-C. Qing, F. Luo and D.-M. Zhu, Effect of Ti_3SiC_2 Addition on Microwave Absorption Property of Ti_3SiC_2/Cordierite Coatings, *Surf. Coat. Tech.*, 2015, **270**, p 39–46.
26. Y.-C. Qing, W.-C. Zhou, F. Luo and D.-M. Zhu, Thin-thickness FeSiAl/flake Graphite-Filled Al_2O_3 Ceramics with Enhanced Microwave Absorption, *Ceram. Int.*, 2017, **43**(1A), p 870–874.
27. D. Zhao, T.-W. Coyle and K. Chien, Phase Composition And Microstructure of Yttrium Aluminum Garnet (YAG) Coatings Prepared by Suspension Plasma Spraying of Y_2O_3-Al_2O_3 Powders, *Surf. Coat. Tech.*, 2013, **235**, p 303–309.
28. D. Zhao, F. Luo, W.-C. Zhou and D.-M. Zhu, Effect of Critical Plasma Spray Parameter on Complex Permittivity and Microstructure by Plasma Spraying Cr/Al_2O_3 Coatings, *appl. Surf. Sci.*, 2013, **264**, p 545–551.
29. S.-J. Penn, N.-M. Alford, A. Templeton, X.-R. Wang, M.-S. Xu, M. Reece and K. Schrapel, Effect of Porosity and Grain Size on the Microwave Dielectric Properties of Sintered Alumina, *J. Am. Ceram. Soc.*, 1997, **80**(7), p 1885–1888.
30. J. Krupka, K. Derzakowski, B. Riddle and J. Baker-Jarvis, A Dielectric Resonator for Measurements of Complex Permittivity of Low Loss Dielectric Materials as a Function of Temperature, *Meas. Sci. Technol.*, 1998, **9**, p 1751–1756.
31. S. Kang, W. Zhang, Z. Hu, J. Yu, Y. Wang and J. Zhu, Porous Core-Shell Zeolitic Imidazolate Framework-Derived Co/NPC@ ZnO-Decorated Reduced Graphene Oxide for Lightweight and Broadband Electromagnetic Wave Absorber, *J. Alloys Compds.*, 2020, **818**, p 152932.
32. L. Wang, S.-Y. Liu, J.-F. Gou, Q.-W. Zhang, F.-F. Zhou, Y. Wang and R.-Q. Chu, Study on the Wear Resistance of Graphene Modified Nanostructured Al_2O_3/TiO_2 Coatings, *Appl. Surf. Sci.*, 2019, **492**, p 272–279.
33. J.-B. Su, W.-C. Zhou, H.-Y. Wang, Y. Liu, Y.-C. Qing, F. Luo, D.-M. Zhu and L. Zhou, Effect of Critical Plasma Spray Parameters on Microstructure and Microwave Absorption Property of Ti_3SiC_2/Cordierite Coatings, *J. Therm. Spray Technol.*, 2016, **25**(4), p 639–649.
34. Y. Zhang, H. Si, S. Liu, Z. Jiang, J. Zhang and C. Gong, Facile Synthesis of BN/Ni Nanocomposites for Effective Regulation of Microwave Absorption Performance, *J. Alloys Compds.*, 2021, **850**, p 156680.
35. J.-B. Su, W.-C. Zhou, Y. Liu, F. Luo and D.-M. Zhu, Atmosphere Plasma-Sprayed Carbon Nanotubes/Cordierite Nanocomposite Coatings for Microwave Absorption Applications, *J. Therm. Spray Technol.*, 2014, **23**(7), p 1065–1072.
36. Y. Liu, X.-W. Yin, L. Kong, X.-M. Liu, F. Ye, L.-T. Zhang and L.-F. Cheng, Electromagnetic Properties of SiO_2 Reinforced with Both Multi-Wall Carbon Nanotubes and ZnO Particles, *Carbon*, 2013, **64**, p 541–544.
37. Z.-N. Yang, W. Ren, L. Zhu, Y.-C. Qing, Z.-B. Huang, F. Luo and W.-C. Zhou, Electromagnetic-Wave Absorption Property of Cr_2O_3-TiO_2 Coating with Frequency Selective Surface, *J. Alloy. Compd.*, 2019, **803**, p 111–117.
38. D. Zhao, F. Luo, W.-C. Zhou and D.-M. Zhu, Microwave absorption Properties and Complex Permittivity of Fe/FeAl2O4 Coatings Deposited by Reactive Plasma Spraying Al/Fe_2O_3 Powders, *Surf. Coat. Tech.*, 2011, **205**(17–18), p 4254–4259.
39. S. Wang, Q. Jiao, X. Liu, Y. Xu, Q. Shi, S. Yue, Y. Zhao, H. Liu, C. Feng and D. Shi, Controllable Synthesis of γ-Fe_2O_3 Nanotube/Porous rGO Composites and Their Enhanced Microwave Absorption Properties, *ACS Sustain. Chem. Eng.*, 2019, **7**(7), p 7004–7013.
40. Z.-N. Yang, F. Luo, Y. Hu, S.-C. Duan, D.-M. Zhu and W.-C. Zhou, Dielectric and Microwave Absorption Properties of TiO_2/Al_2O_3 Coatings and Improved Microwave Absorption by FSS Incorporation, *J. Alloy. Compd.*, 2016, **678**, p 527–532.
41. D. Zhao, F. Luo, W. Zhou and D. Zhu, Complex Permittivity and Microwave-Absorbing Properties of Fe/Al_2O_3 Coatings by Air Plasma Spraying Technique, *Int. J. App. Ceram. Technol.*, 2013, **10**, p E88–E97.
42. L. Zhou, G.-X. Su, H.-B. Wang, J.-L. Huang, Y.-J. Guo, Z. Li and X.-H. Su, Influence of NiCrAlY Content on Dielectric and Microwave Absorption Properties of NiCrAlY/Al_2O_3 Composite Coatings, *J. Alloy. Compd.*, 2019, **777**, p 478–484.
43. D. Chen, F. Luo, W.-C. Zhou and D.-M. Zhu, Effect of Ti_3SiC_2 Addition on Microwave Absorption Property of Plasma Sprayed

Ti_3SiC_2/NASICON Coatings, *J. Mater. Sci-mater. El.*, 2018, **29**(16), p 13534–13540.

44. A.-M. Bu, Y.-F. Zhang, Y. Xiang, W.-W. Chen, H.-W. Cheng and L. Wang, Enhanced Antioxidation and Microwave Absorbing Properties of SiC/SiO_2 Coating on Carbon Fiber, *J. Mater. Sci-mater. El.*, 2020, **31**(19), p 17067–17074.
45. Q.-L. Wen, W.-C. Zhou, J.-B. Su, Y.-C. Qing, F. Luo and D.-M. Zhu, Dielectric and Microwave Absorption Properties Of Plasma Sprayed Short Carbon Fibers/Glass Composite Coatings, *J. Mater. Sci-mater. El.*, 2016, **27**(2), p 1783–1790.